



A New Virtual Oscillator Control Without Third-Harmonics Injection For DC/AC Inverter

Luo, Siyi; Wu, Weimin; Koutroulis, Eftichios; Chung, Henry Shu-hung; Blaabjerg, Frede

Published in:
I E E Transactions on Power Electronics

DOI (link to publication from Publisher):
[10.1109/TPEL.2021.3066162](https://doi.org/10.1109/TPEL.2021.3066162)

Publication date:
2021

Document Version
Accepted author manuscript, peer reviewed version

[Link to publication from Aalborg University](#)

Citation for published version (APA):
Luo, S., Wu, W., Koutroulis, E., Chung, H. S., & Blaabjerg, F. (2021). A New Virtual Oscillator Control Without Third-Harmonics Injection For DC/AC Inverter. *I E E Transactions on Power Electronics*, 36(9), 10879 - 10888. [9380509]. <https://doi.org/10.1109/TPEL.2021.3066162>

General rights

Copyright and moral rights for the publications made accessible in the public portal are retained by the authors and/or other copyright owners and it is a condition of accessing publications that users recognise and abide by the legal requirements associated with these rights.

- Users may download and print one copy of any publication from the public portal for the purpose of private study or research.
- You may not further distribute the material or use it for any profit-making activity or commercial gain
- You may freely distribute the URL identifying the publication in the public portal -

Take down policy

If you believe that this document breaches copyright please contact us at vbn@aub.aau.dk providing details, and we will remove access to the work immediately and investigate your claim.

A New Virtual Oscillator Control without Third-Harmonics Injection for DC/AC Inverter

Siyi Luo, Weimin Wu, *Member, IEEE*, Eftichios Koutroulis, *Senior Member, IEEE*, Henry Shu-Hung Chung, *Fellow, IEEE*, and Frede Blaabjerg, *Fellow, IEEE*

Abstract—Virtual Oscillator Control (VOC) is a type of nonlinear grid-forming controller for DC/AC inverters. Compared with the droop control method, the original VOC has a faster transient response in islanded mode. However, its output voltage always contains a third-order harmonic, resulting in a significant third-harmonic current, especially in the grid-connected mode. In order to eliminate this harmonic, a notch-type filter is typically employed, but it affects the synchronization speed of multiple DC/AC inverters connected in parallel in islanded mode. In this paper, by analyzing the nonlinear dynamical equations of the oscillator and simplifying its nonlinear current source, a novel VOC for three-phase DC/AC inverters is proposed, which can successfully eliminate the third-order harmonic in the output voltage of the oscillator. Further, compared with the traditional VOC with notch filter, the grid-synchronization response of the proposed VOC-based DC/AC inverters can be significantly improved. A 3 kW/3-phase/120 V experimental prototype system designed on the DSPACE DS1202 platform has been developed to verify the feasibility of the proposed control strategy.

Index Terms—Microgrids, virtual oscillator control, harmonic elimination, grid synchronization.

I. INTRODUCTION

Distributed power generation (DG) together with Renewable Energy, such as photovoltaic and wind power sources, has received a lot of attention recently [1]–[2]. DG units play a significant role in improving the power quality and reducing the transmission losses of electric power systems. The majority of distributed power generation sources require power electronic DC/AC inverters (voltage-source inverters) to interface them into the grid through a line at the point of common coupling (PCC). In grid-forming control, the control object of the voltage source inverter is the output voltage of the inverter, instead of the grid-injected current. Microgrids

typically contain multiple DC/AC inverters connected in parallel to an AC bus. Therefore, the overall system of DC/AC inverters must support and maintain the voltage and frequency of the microgrid. Droop control is a well-established method that is applied for interfacing grid-tied inverters in AC microgrids. The target of droop control is to emulate the droop external characteristics of virtual synchronous machines (VSMs), which achieve power balance by allowing a deviation from the nominal voltage and frequency [3]–[6]. In a resistance dominated network, the active power is closely related to the voltage amplitude, while the reactive power is related to the phase angle [7]–[8].

Virtual oscillator control (VOC) is an emerging advanced decentralized control method that can simulate the dynamic characteristics of limit-cycle oscillators [9]–[11], such as the Van der Pol oscillator. VOC has been applied to a single-phase microgrid in ref. [13] and a three-phase microgrid in ref. [14]. In ref. [13], a nonlinear analysis method was used to prove the global asymptotic synchronization of the virtual oscillator in an islanded microgrid. The analysis presented in [15]–[16] demonstrates that a virtual-oscillator-controlled inverter exhibits a droop-like behavior. In ref. [17], the comprehensive requirement for the synchronization of grid-tied inverters with VOC was presented in details. In order to achieve a seamless control of active and reactive power, an additional power loop was introduced into the VOC in order to track the reference power set-point [18]–[20]. In [21]–[22], a complex-valued parameter was introduced into the VOC to realize the independent control of active and reactive power. The dispatchable VOC methods (also named as dVOC) were recently reported in [23]–[25]. Through the local measurement and power set-points, dVOC can generate the grid-forming behavior and change the power generation without an additional power loop. The transient stability of a grid-connected inverter controlled by a dispatchable virtual oscillator has been evaluated in [26]. The virtual oscillator control of distributed power filters for selective ripple attenuation was introduced in [27].

A salient advantage of VOC is that the virtual oscillator is a time-domain controller that reacts to the instantaneous current without additional filters or power calculations. It exhibits a fast response during transients and stabilizes the dynamic response [28]–[29]. Compared with the droop control technique, the amplitude synchronization speed can be significantly improved. Although VOCs exhibit very good dynamic response in islanded microgrids, their utilization is still limited, due to the lack of compatible grid synchronization techniques and the existence of the third harmonic at the oscillator output voltage [30]. In ref. [30], a comprehensive hierarchical control method has been applied to the conventional VOC-based single-phase inverter to reduce the error introduced by the primary control. In that case, the third harmonic of the oscillator output voltage was eliminated by an additional notch filter. However, the synchronization speed is affected by this notch filter in the

Manuscript received August 7, 2020; revised November 3, 2020; revised December 13, 2020; accepted January 9, 2021. Date of publication; date of current version. This work was supported in part by the National Natural Science Foundation of China under Grant 51877130, in part by the National Key Research and Development Project of China under Grant 2017YFGH001164 and in part by the program “Bilateral and Multilateral Research & Technology Co-operation between Greece and China” under Grants 2017YFGH001164 and eSOLAR/T7ΔKI-00066. Recommended for publication by Associate Editor *****. (Corresponding author: Weimin Wu.)

W. Wu and Z. Zhao are with the Electrical Engineering Department, Shanghai Maritime University, Shanghai 201306, China (e-mail: wmwu@shmtu.edu.cn; 201830210047@stu.shmtu.edu.cn).

E. Koutroulis is with the School of Electrical and Computer Engineering, Technical University of Crete, Chania 73100, Greece (e-mail: efkout@electronics.tuc.gr).

H. S.-H. Chung is with the Department of Electrical Engineering and the Centre for Smart Energy Conversion and Utilization Research, City University of Hong Kong, Hong Kong (e-mail: eeshc@cityu.edu.hk).

F. Blaabjerg is with the Energy Engineering Department, Aalborg University, Aalborg 9100, Denmark (e-mail: fbj@et.aau.dk).

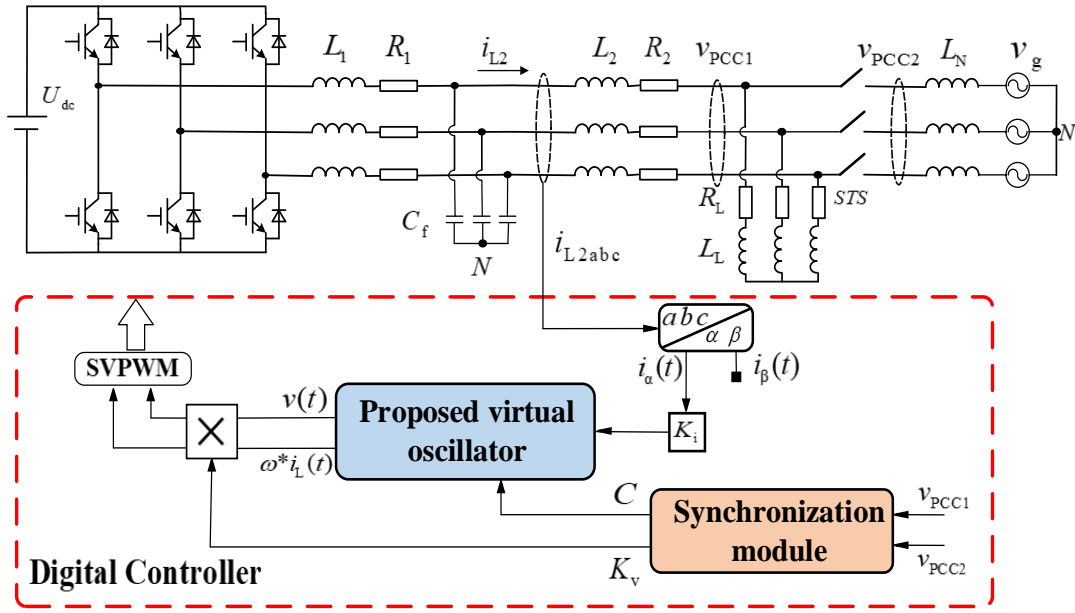


Fig. 1. The proposed VOC-based three-phase DC/AC inverter.

islanded mode of operation. In ref. [31]-[33], a grid-compatible oscillator based on the Andronov-Hopf dynamic response was also proposed to eliminate the third harmonic. Nevertheless, the Andronov-Hopf-based oscillator is designed for three-phase system. Applying it to single-phase systems requires further research.

In this paper, a novel VOC for DC/AC inverters is proposed to eliminate the third-harmonic voltage of the traditional one, without affecting its droop characteristics. Compared with the traditional VOC [15], the response speed of proposed VOC-based DC/AC inverters can be significantly improved. Compared with the traditional VOC with notch filter [30], the proposed VOC can successfully suppress the third harmonic, without affecting the synchronization speed under different initial conditions in the islanded mode of operation.

The rest of the paper is organized as follows: firstly, in Section II, the three-phase inverter based on VOC is introduced, and the disadvantages of the traditional VOC-based inverters are analyzed. Then, in Section III, based on the analysis of the traditional VOC, a novel virtual oscillator is proposed, which can eliminate the third harmonic without affecting the response speed, while the corresponding grid-connected synchronization measures are also introduced. In Section IV, the effectiveness of the proposed VOC controller is demonstrated using a 3 kW / three-phase four-wire / 120 V experimental prototype system. Finally, the conclusion is summarized and the future potential is discussed in Section V.

II. BASIC MODEL OF VOC-BASED THREE-PHASE DC/AC Inverters

In this section, the comprehensive average dynamic equations of three-phase four-wire DC/AC inverters based on a VOC are derived. It is also shown that there is a trade-off between the dynamic response of the oscillator and the harmonic voltage.

A. Original VOC-based Three-phase Inverters

Fig. 1 illustrates that the VOC-based four-line three-phase DC/AC inverter is connected with the local RL load and the power grid through an LCL filter and a static transfer switch

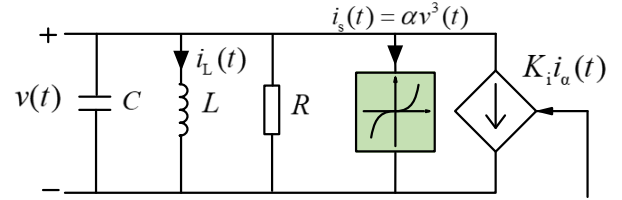


Fig. 2. The traditional virtual oscillator.

(STS). The LCL-filter is designed based on the rule given in ref. [34]. The DC link voltage is symbolized as U_{dc} . The inductor current and the grid phase voltage are symbolized as i_{L2} and v_g , respectively. The voltages at the PCCs are symbolized as v_{PCC1} and v_{PCC2} , respectively. The current feedback gain and the voltage scaling factor of the oscillator are symbolized as K_i and K_v , respectively. The parameters L_1 and L_2 are the inverter-side inductor and the grid-side inductor of the LCL filter, respectively, while R_1 and R_2 are the parasitic resistors of these two inductors. It is noted that C_f denotes the capacitor between the two inductors. Also, L_N correspond to the inductance of the electric grid lines. The local load resistor and inductor are symbolized as R_L and L_L , respectively.

In a VOC-based three-phase inverter, the design of the controller can be simplified through the coordinate transformation [6]. In this paper, the controller is designed in the $\alpha\beta$ frame, where i_{L2abc} is the output current of the three-phase inverter. The α - and β - components of i_{L2abc} after coordinate transformation are defined as $i_\alpha(t)$ and $i_\beta(t)$, where only $i_\alpha(t)$ is provided as input to the proposed VOC.

Fig. 2 illustrates the structure of a traditional virtual oscillator. It is noted that L and C are the oscillator inductor and the oscillator capacitor, respectively. The oscillator resistor is symbolized as R , where $R = -1/\sigma$. The oscillator current source is represented as $i_s(t)$, where α is a positive constant of the oscillator current source. The current flowing through inductor L is denoted as $i_L(t)$, and $v(t)$ is the output voltage of the oscillator. The nonlinear equations of VOC are the following:

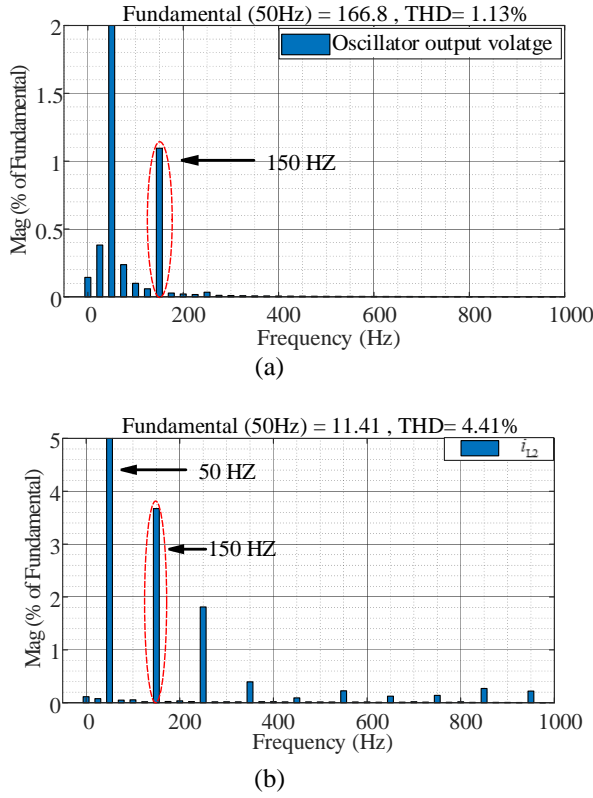


Fig. 3. FFT spectrum of a traditional virtual oscillator: (a) oscillator output voltage $v(t)$, and (b) inductor current i_{L2} .

$$L \frac{di_L(t)}{dt} = v(t) \quad (1)$$

$$C \frac{dv(t)}{dt} = -i_s(t) + \sigma v(t) - i_L(t) - K_i i_a(t) \quad (2)$$

The output voltage of the oscillator is given by

$$v(t) = \sqrt{2}V_{RMS}(t) \cos(\omega t + \theta(t)) \quad (3),$$

where

$$V_{RMS}(t) = \left(\frac{\sigma \pm \sqrt{\sigma^2 - 6\alpha K_i / K_v \bar{P}(t)}}{3\alpha} \right)^{\frac{1}{2}} \quad (4)$$

$$\omega = \omega^* + \frac{K_i K_v \bar{Q}(t)}{2C V_{RMS}^2(t)} \quad (5)$$

and $V_{RMS}(t)$ is the RMS voltage over one line frequency cycle, while the oscillator output voltage frequency and phase offset are symbolized as ω and $\theta(t)$. The parameter of ω^* is the nominal frequency of the inverter. It is noted that $\bar{P}(t)$ and $\bar{Q}(t)$ correspond to the average real and reactive power outputs of the VO-controlled inverter at the switch terminals over an ac cycle of period $2\pi/\omega^*$ [15]. The detailed derivation of (4) and (5) is given in Section III-A.

The droop characteristic of the traditional VOC can be written as follows

$$V_{RMS}(t) = V_{oc} + m_p \bar{P}(t) \quad (6)$$

$$\omega = \omega^* + m_Q \bar{Q}(t) \quad (7),$$

where m_p and m_Q are the equivalent droop coefficients of VOC and $V_{oc} = K_v \sqrt{2\sigma/3\alpha}$ is the open circuit voltage of the oscillator, which can be obtained by substituting $\bar{P} = 0$ in (4).

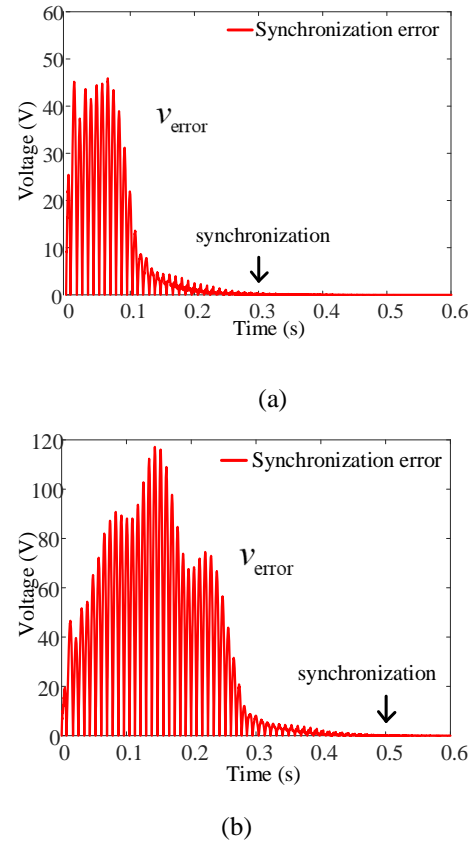


Fig. 4. Synchronization error in the islanded mode of operation: (a) traditional VOC, (b) traditional VOC with notch filter.

The values of m_p and m_Q can be obtained by deriving (4) and (5) as:

$$m_p = \frac{K_i}{2\sigma K_v} \frac{1}{V_{RMS}(t) - \beta V_{RMS}^3(t)} \quad (8)$$

$$m_Q = \frac{K_i K_v}{2C V_{RMS}^2(t)} \quad (9)$$

B. Third-Order Harmonic Caused by the Original Traditional VOC

In ref. [15], the perturbation methods and the method of multiple scales [35] were used to analyze the harmonic content in the oscillator. The output voltage of the oscillator is given as follows:

$$v(\tau_0, \varepsilon) \approx \sqrt{2} \cos(\tau_0 + \theta_0) - \frac{\varepsilon \sigma \sqrt{2}}{8} \sin(3\tau_0 + 3\theta_0) \quad (10)$$

where $\varepsilon = \sqrt{L/C}$. The original time scale is denoted as τ_0 , and $\tau_1 = \varepsilon \tau_0$ is the slower time scale. It is noted that v is composed of the fundamental wave and the third-harmonic components.

The FFT spectrum of the oscillator output voltage is shown in Fig. 3 (a). It is observed that the output voltage of the traditional VOC has an undesirable third harmonic component (almost 1 %). In the grid-connected mode, the third-harmonic voltage in the output voltage of the oscillator will also generate a larger third-harmonic current in the grid-side current. As shown in Fig. 3 (b), the third-harmonic in the grid-side current i_{L2} is close to 4%, which will severely deteriorate the power quality of the electric grid.

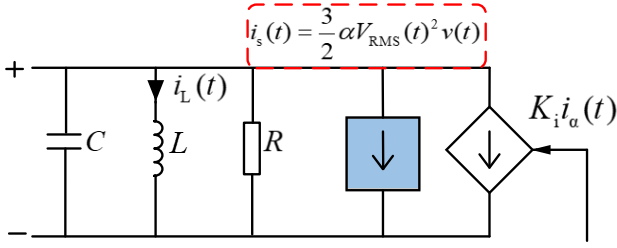


Fig. 5. The proposed virtual oscillator.

The relative amplitude of the third-harmonic component to the fundamental is defined as $\delta_{3:1}$, and the rise time of the oscillator is defined as t_{rise}

$$\delta_{3:1} = \frac{\varepsilon\sigma}{8}, t_{\text{rise}} = \frac{6}{\omega^* \varepsilon\sigma} \quad (11).$$

It is concluded that the undesirable third-harmonic is directly proportional to $\varepsilon\sigma$, and the rise time t_{rise} of the oscillator is inversely proportional to $\sigma\varepsilon$. Reducing the third-harmonic component by selecting appropriate parameters will inevitably affect the transient response [15].

C. Effect on the Synchronization Speed of the Traditional VOC with Notch Filter

To the best of the authors' knowledge, only a notch filter (12) has been employed to eliminate the third harmonic of the oscillator output voltage [30]. However, the notch filter should not be used in the islanded mode of operation because it may affect the synchronization speed of the oscillator.

$$H_{\text{NF}}(s) = \sum_{h=3} \frac{s^2 + 2\zeta_1(h\omega_0)s + (h\omega_0)^2}{s^2 + 2\zeta_2(h\omega_0)s + (h\omega_0)^2} \quad (12),$$

where $\zeta_1 < \zeta_2$, $\omega_0 = 100\pi$ and h denotes the harmonic order.

Figs. 4 (a) and (b) illustrate the time required by two parallel-connected inverters controlled by the traditional VOC and the traditional VOC with notch filter, respectively, to synchronize from arbitrarily different initial conditions. The synchronization error v_{error} can be defined as:

$$v_{\text{error}} = |v_1 - v_2| \quad (13),$$

where v_1 and v_2 are the output voltages of inverter #1 and inverter #2, respectively.

It is observed that the synchronization time of the traditional VOC is less than 0.3 s, but the synchronization time of the traditional VOC with notch filter is approximately 0.5 s. Therefore, it is concluded that the notch filter will undoubtedly affect the synchronization speed of multiple DC/AC inverters connected in parallel.

III. PROPOSED VIRTUAL OSCILLATOR AND ITS CHARACTERISTICS

In this section, an improved VOC is proposed, which is obtained by improving the nonlinear current source of the oscillator. Thus, it is capable to achieve better dynamic characteristics and a reduction of the third-order harmonic component.

A. Proposed Virtual Oscillator

In a traditional virtual oscillator, the nonlinear current source is a cubic function of the oscillator output voltage

$$i_s(t) = \alpha v^3(t) = 2\sqrt{2}\alpha V_{\text{RMS}}^3(t) \cos^3(\omega t + \theta(t)) \quad (14).$$

By applying trigonometric identities, it is obtained that

$$\cos^3(x) = \frac{3}{4}\cos(x) + \frac{1}{4}\cos(3x) \quad (15)$$

From (14), it can be derived that $\cos(3x)$ is the cause of the third-harmonic voltage, so it is ignored when constructing a nonlinear current source. Therefore, the non-linear current source of the oscillator can be changed to

$$\begin{aligned} i_s(t) &= \alpha v^3(t) = 2\sqrt{2}\alpha V_{\text{RMS}}^3(t) \cdot \frac{3}{4}\cos(x) \\ &= \frac{3}{2}\alpha V_{\text{RMS}}^2(t) \cdot v(t) \end{aligned} \quad (16).$$

Substituting (16) in (1) and (2) results in

$$\begin{aligned} C \frac{d^2 v(t)}{dt^2} &= -\alpha \frac{3}{2} V_{\text{RMS}}^2(t) \cdot \frac{dv(t)}{dt} + \sigma \frac{dv(t)}{dt} - \frac{di_L(t)}{dt} \\ &\quad - K_i \frac{di_a(t)}{dt} \end{aligned} \quad (17)$$

Fig. 5 shows the equivalent circuit of the proposed virtual oscillator. Note that in digital control, the proposed virtual oscillator is realized with the mathematical model of the improved nonlinear equation (17), so as to change the VOC parameters in real time.

B. Droop Characteristic

A VOC is a time-domain controller that can emulate a droop-like behavior, where the droop form of response is inherent in the nonlinear nature of the oscillator. The improvement of the nonlinear current source does not affect its droop characteristics.

Considering the equivalent circuit of Fig. 5, the dynamics of the proposed virtual-oscillator inductor current of i_L , and oscillator output voltage of v , are given by

$$L \frac{di_L(t)}{dt} = v(t) \quad (18)$$

$$C \frac{dv(t)}{dt} = -\alpha \frac{3}{2} V_{\text{RMS}}^2(t) \cdot v(t) + \sigma v(t) - i_L(t) - K_i i_a(t) \quad (19)$$

Substituting (3) in (18) results in

$$\varepsilon^* i_L(t) = \sqrt{2} V_{\text{RMS}}(t) \sin(\omega t + \theta(t)) \quad (20)$$

Next, with the coordinate transformation

$$\begin{aligned} \sqrt{2} V_{\text{RMS}}(t) &= \sqrt{(\varepsilon^* i_L(t))^2 + v^2(t)}, \\ \omega t + \theta(t) &= \tan^{-1} \left(\frac{\varepsilon^* i_L(t)}{v(t)} \right) \end{aligned} \quad (21)$$

applied to (18) and (19), the evolution of $V_{\text{RMS}}(t)$ and $\theta(t)$ can be expressed as:

$$\begin{aligned} \frac{dV_{\text{RMS}}(t)}{dt} &= \frac{1}{\sqrt{2}C} \sigma (v(t) - \frac{\beta}{2} V_{\text{RMS}}^2(t) \cdot v(t)) \cos(\omega t + \theta(t)) \\ &\quad - \frac{1}{\sqrt{2}C} K_i i_a(t) \cos(\omega t + \theta(t)) \end{aligned} \quad (22)$$

$$\begin{aligned} \frac{d\theta(t)}{dt} &= \omega^* - \omega - \frac{\sigma}{\sqrt{2} V_{\text{RMS}}(t) C} (v(t) \sin(\omega t + \theta(t)) \\ &\quad - \frac{\beta}{2} V_{\text{RMS}}^2(t) \cdot v(t) \sin(\omega t + \theta(t))) \\ &\quad - \frac{1}{\sqrt{2} V_{\text{RMS}}(t) C} K_i i_a(t) \sin(\omega t + \theta(t)) \end{aligned} \quad (23)$$

where $\beta=3\alpha/\sigma$. The dynamic response expressed by (22) and (23) is then averaged over $2\pi/\omega$, resulting in the following nonlinear differential equations

$$\begin{aligned} \frac{d\bar{V}_{\text{RMS}}(t)}{dt} &= \frac{\sigma}{2\pi C\sqrt{2}} \int_0^{2\pi} v(t) \cos(\omega t + \bar{\theta}(t)) - \frac{\beta}{2} \bar{V}_{\text{RMS}}^2(t) * v(t) \cos(\omega t + \bar{\theta}(t)) \\ &\quad - \frac{K_i}{\sigma} i_a(t) \cos(\omega t + \bar{\theta}(t)) dt \\ &= \frac{\sigma}{2C} (\bar{V}_{\text{RMS}}(t) - \frac{\beta \bar{V}_{\text{RMS}}^3(t)}{2}) - \frac{K_i K_v}{2C \bar{V}_{\text{RMS}}(t)} \bar{P}(t) \end{aligned} \quad (24)$$

$$\begin{aligned} \frac{d\bar{\theta}(t)}{dt} &= \omega^* - \omega - \int_0^{2\pi} \left(\frac{\bar{V}_{\text{RMS}}(t) \cos(\omega t + \bar{\theta}(t)) \sin(\omega t + \bar{\theta}(t))}{2\pi C \bar{V}_{\text{RMS}}(t)} \right. \\ &\quad \left. + \frac{\beta \bar{V}_{\text{RMS}}^3(t)}{4\pi C \bar{V}_{\text{RMS}}(t)} \cos(\omega t + \bar{\theta}(t)) \sin(\omega t + \bar{\theta}(t)) \right) dt \\ &\quad + \frac{K_i}{4\pi C \bar{V}_{\text{RMS}}(t)} \int_0^{2\pi} \sqrt{2} i_a(t) \sin(\omega t + \bar{\theta}(t)) dt \\ &= \omega^* - \omega + \frac{K_i K_v}{2C \bar{V}_{\text{RMS}}^2(t)} \bar{Q}(t) \end{aligned} \quad (25)$$

where $\bar{V}_{\text{RMS}}(t)$ is the average value of $V_{\text{RMS}}(t)$ in an AC cycle, and $\bar{P}(t)$ and $\bar{Q}(t)$ correspond to the average active and reactive, respectively, power output at the inverter terminals. The equilibrium solution of (24) and (25) is given by

$$\bar{V}_{\text{RMS}}(t) = \left(\frac{\sigma \pm \sqrt{\sigma^2 - 6\alpha K_i/K_v \bar{P}(t)}}{3\alpha} \right)^{\frac{1}{2}} \quad (26)$$

$$\omega = \omega^* + \frac{K_i K_v \bar{Q}(t)}{2C \bar{V}_{\text{RMS}}^2(t)} \quad (27)$$

The maximum frequency of ω is $(1+5\%)\omega^*$. Obviously, the steady-state equilibrium solution of the proposed VOC is the same as the traditional VOC. Therefore, the same droop characteristics as the traditional VOC can be obtained. Also, (26) can be written as follows

$$V_{\text{RMS}}(t) * K_v = V_{\text{oc}} + m_p P(t) \quad (28),$$

where $V_{\text{oc}} = K_v \sqrt{2\sigma/3\alpha}$ and m_p is the active-power droop coefficient

$$m_p = \frac{K_i}{2\sigma K_v} \frac{1}{V_{\text{RMS}}(t) - \beta V_{\text{RMS}}^3(t)} \quad (29).$$

The same droop-like behavior is also shown in the frequency evolution equation as

$$\omega = \omega^* + m_Q Q(t) \quad (30),$$

where m_Q is the reactive-power droop coefficient:

$$m_Q = \frac{K_i K_v}{2C \bar{V}_{\text{RMS}}^2(t)} \quad (31)$$

It is not difficult to detect that the improvement of the oscillator's nonlinear current source will not affect its droop characteristics.

C. Elimination of Third-Order Harmonic

In this part, the harmonic content in the proposed VOC is analyzed by the multiple scales and perturbation methods [35]. Considering the case of a virtual oscillator not connected to the inverter, then (17) can be rewritten in the time coordinates $\tau = \omega^* t = (1/\sqrt{LC})t$ as follows:

$$\ddot{v} - \varepsilon \left(\sigma - \frac{3}{2} \alpha V_{\text{RMS}}^2 \right) \dot{v} + v = 0 \quad (32)$$

where $\varepsilon \rightarrow 0$.

Using a regular perturbation expansion, it can be assumed that the approximate solution of the above equation can be decomposed into the sum of components on multiple time scales

$$v(\tau_0, \varepsilon) \approx v_0(\tau_0, \tau_1) + \varepsilon v_1(\tau_0, \tau_1) \quad (33)$$

where τ_0 is the original time scale and $\tau_1 = \varepsilon \tau_0$ is the slower time scale.

Substituting (33) in (32) results in

$$\left(\frac{\partial^2 v_0}{\partial \tau_0^2} + v_0 \right) + \varepsilon \left(\frac{\partial^2 v_1}{\partial \tau_0^2} + v_1 + 2 \frac{\partial^2 v_0}{\partial \tau_0 \partial \tau_1} - \sigma \left(1 - \frac{3}{2} \alpha V_{\text{RMS}}^2 \right) \frac{\partial v_0}{\partial \tau_0} \right) = 0 \quad (34)$$

In order for the equation to be true, the terms in the brackets need to be equal to 0:

$$\frac{\partial^2 v_0}{\partial \tau_0^2} + v_0 = 0 \quad (35)$$

$$\Rightarrow v_0(\tau_0, \tau_1) = a(\tau_1) \cos(\tau_0 + \theta(\tau_1))$$

where v_0 can be considered as the approximate fundamental component of the oscillator output voltage, while $a(\tau_1)$ and $\theta(\tau_1)$ are the amplitude and phase terms of the voltage.

Substituting (35) into (34) results in:

$$\begin{aligned} \frac{\partial^2 v_1}{\partial \tau_0^2} + v_1 &= \left(2 \frac{\partial a(\tau_1)}{\partial \tau_1} - \sigma a(\tau_1) + \frac{3\alpha V_{\text{RMS}}^2 a(\tau_1)}{2} \right) \sin(\tau_0 + \theta(\tau_1)) \\ &\quad + 2a \frac{\partial \theta(\tau_1)}{\partial \tau_1} \cos(\tau_0 + \theta(\tau_1)) \end{aligned} \quad (36)$$

The lower time scales of v_1 in the traditional VOC are expressed as follows [15]:

$$\begin{aligned} \frac{\partial^2 v_1}{\partial \tau_0^2} + v_1 &= \left(2 \frac{\partial a(\tau_1)}{\partial \tau_1} - \sigma a(\tau_1) + \frac{\sigma}{2} a^3(\tau_1) \right) \sin(\tau_0 + \theta(\tau_1)) \\ &\quad + 2a(\tau_1) \frac{\partial \theta(\tau_1)}{\partial \tau_1} \cos(\tau_0 + \theta(\tau_1)) \\ &\quad + \frac{\sigma}{2} a^3(\tau_1) \sin(3\tau_0 + 3\theta(\tau_1)) \end{aligned} \quad (37)$$

It can be inferred from (36) and (37) that by replacing the nonlinear current source of the oscillator, the approximate solution on lower time scales in the proposed VOC does not contain the third-harmonic term.

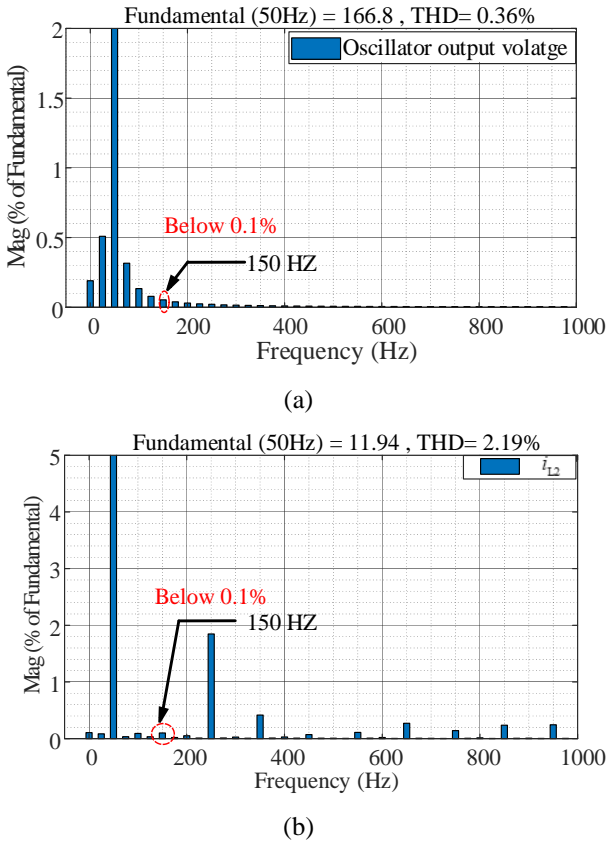


Fig. 6. FFT spectrum of the proposed VOC inductor current i_{L2} : (a) oscillator output voltage $v(t)$, and (b) inductor current i_{L2} .

The value of v_1 of the proposed VOC can be deduced as follows

$$v_1 = a_1 \cos(\tau_1 + \theta_1) \quad (38)$$

and the value of v_1 of the traditional VOC is given by

$$v_1 = -\frac{\sigma}{4\sqrt{\beta}} \sin(3\tau_0 + \theta_0) \quad (39)$$

The expressions in (38) and (39) indicate that the unwanted third-harmonic component will not appear in the proposed VOC, but it exists in the traditional VOC. Considering that τ_1 is the slower time scale, the term v_1 of the proposed VOC has almost no effect on the steady-state solution of v .

Fig. 6 (a) shows that by using the proposed method, the third-harmonic component in the oscillator output voltage is significantly reduced. In grid-tied operation, the FFT spectrum of the inductor current i_{L2} is shown in Fig. 6 (b). By using the proposed VOC, the third-harmonic component in the grid-side current is reduced from 4 % to 0.2 %, which greatly improves the waveform of the grid-injected current and makes the DC/AC inverter more securely connected to the grid. It is worth noting that, according to (4) and (5), the appropriate values of the operating parameters can be selected in the proposed oscillator in order to achieve a faster response speed.

D. Synchronization Speed Analysis in the Off-line Mode

The notch filter cannot be used in the islanded mode of operation because it will affect the synchronization speed of the oscillator.

Fig. 7 shows the synchronization error of the proposed VOC in the islanded mode, where it can be seen that the

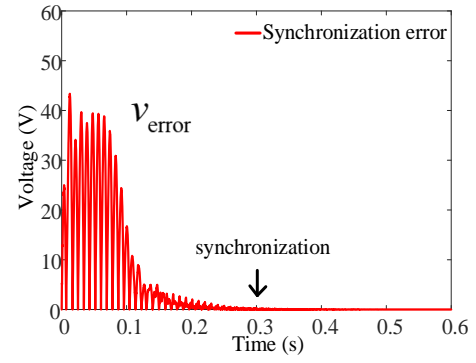


Fig. 7. Synchronization error of the proposed VOC in islanded mode.

synchronization speed of the proposed VOC is less than 0.3 s. In Fig. 4 (a), the synchronization speed of the traditional VOC is also 0.3 s. After the inverters are synchronized, multiple parallel-connected inverters can realize the even distribution of the load power.

Therefore, when the initial conditions of the oscillator capacitors of the parallel inverters are different, the synchronization time of the inverter with the notch filter will increase, while the proposed oscillator will not affect the synchronization time of the overall system.

E. Grid-Synchronization Measures

In the islanded mode, the droop characteristics of the VOC will cause the amplitude and phase of the voltage at the PCC to deviate from their nominal values. Hence, when a VOC-based inverter directly switches from the islanded mode to the grid-tied mode, a high inrush current will be generated. Therefore, before connecting the islanded microgrid to the power grid, some certain grid synchronization measures must be addressed to ensure that the microgrid voltage is synchronized with the grid voltage.

Since $\omega^* = \sqrt{L/C}$, by modifying either L or C in the oscillator will also regulate ω^* . Based on this, an adaptive integrator PI compensator is introduced to modify the nominal frequency ω^* in order to achieve closed-loop phase/frequency tracking. The value of C is changed according to the phase difference $e_\theta = \theta_{PCC2} - \theta_{PCC1}$, where θ_{PCC2} and θ_{PCC1} are estimated by using a Phase-Locked Loop (PLL) on v_{PCC2} and v_{PCC1} , respectively. PLL is only used prior to closing the breaker and not for grid-tied operation.

Equation (40) is used to generate C_θ for modifying the capacitance C in (41) as follows

$$C_\theta = (K_p^\theta + \frac{1}{\tau e_\theta^2 + 1})e_\theta \quad (40)$$

$$C = C^* + C_\theta \quad (41)$$

where C^* is the nominal value of the oscillator capacitor. K_p^θ and τ are the proportional constant and variable integral factor, respectively.

The PI compensator is used to adjust the voltage scaling factor K_v and thereby to modify the output voltage amplitude of the oscillator. The value of K_v is changed according to the amplitude difference $e_v = v_{PCC2} - v_{PCC1}$ as follows

$$u_v = (K_p^v + \frac{K_i^v}{s})e_v \quad (42)$$

$$K_v = K_v^* + u_v \quad (43)$$

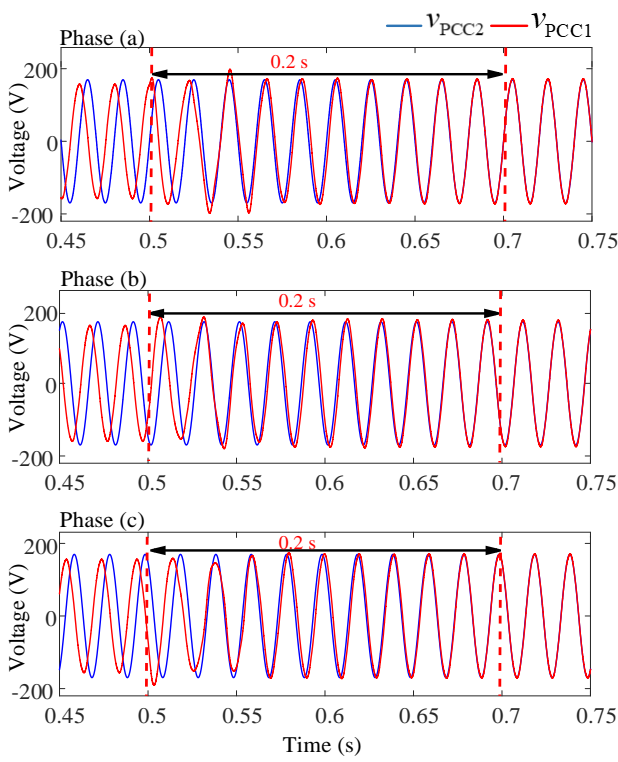


Fig. 8. Three phase PCC2 voltage of v_{PCC2} and PCC1 voltage of v_{PCC1} during grid synchronization.

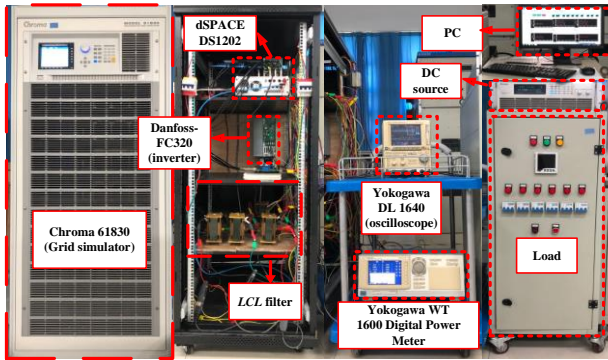


Fig. 9. Experimental setup with a 3 kW/3-phase/110V GCI.

where K_v^* is a coefficient equal to the nominal value of the output voltage, while K_p^v and K_i^v are the proportional and integral, respectively, coefficients of the PI compensator.

In order to verify the grid synchronization capability of the proposed VOC-based three-phase DC/AC inverters shown in Fig. 1, a simulation process was also carried out. The PCC1 voltage of v_{PCC1} and the PCC2 voltage of v_{PCC2} in the grid synchronization mode are shown in Fig. 8. Before 0.5 s, the inverter is operating in the islanded mode. The synchronization module was activated at 0.5 s, and the amplitude and phase errors were eliminated within 0.2 s, thereby achieving synchronized operation. After 0.7 s, the inverter can be safely connected to the electrical grid.

IV. EXPERIMENTAL VERIFICATION

In order to verify the theoretical analysis and demonstrate the effectiveness of the proposed method, a 3 kW/ three-phase four-wire /120V LCL-filter-based experimental prototype with the proposed control method has been implemented by using the dSPACE DS1202 platform, which is shown in Fig. 9. The Chroma 61830 three-phase grid simulator has been used to simulate a three-phase grid. The

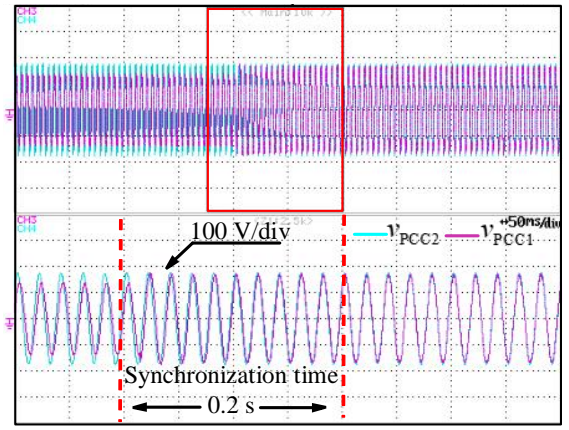
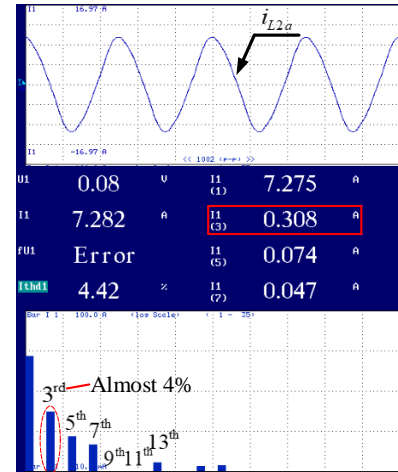
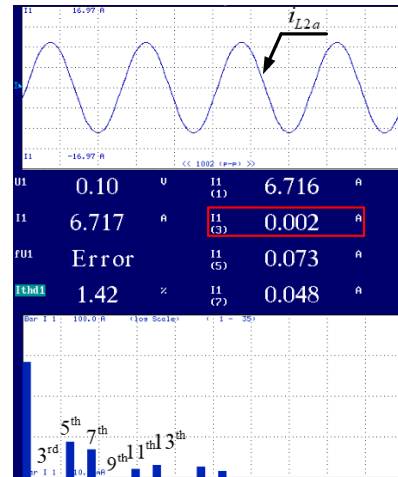


Fig. 10. Voltages on both ends of STS. Scale: voltage – 100V/div, time – 5 ms/div.



(a)



(b)

Fig. 11. Harmonic distortion in grid-side current i_{L2a} : (a) traditional VOC, and (b) the proposed VOC.

Yokogawa DL 1640 digital oscilloscope has been used to measure the grid voltage and grid-side current waveforms. The values of critical parameters are listed in Tables I and II, respectively.

A. Grid Synchronization Operation

As shown in Fig. 10, when the inverter is operating in an off-grid state, significant amplitude and phase differences are developed between v_{PCC1} and v_{PCC2} . The grid-synchronization measures are used to eliminate these amplitude and phase differences. After about 0.2 s, the voltage and phase of v_{PCC1}

and v_{PCC2} are completely matched, and the DC/AC inverter can be safely connected to the power grid.

B. Harmonic Elimination

The YOKOGAWA WT1600 Digital Power Meter has been used to validate the proposed harmonic suppression strategy. As shown in Fig. 11 (a), when the traditional VOC-controlled inverter operates in the grid-connected mode, undesirable third-order harmonics will appear in the grid-side current i_{L2a} . The RMS value of i_{L2a} is 7.282 A, where the third-harmonic content is 0.308 A (almost 4 %), the fifth harmonic content is 0.074 A (almost 1 %), and the seventh harmonic content is 0.047 A (below 1 %). Fig. 11 (b) shows the harmonic content of the grid-side current i_{L2a} in the grid-connected operating mode of the proposed VOC. Obviously, it can be found that the third-order harmonic component in the grid-side current i_{L2a} is significantly reduced. The proposed VOC can effectively reduce the third-harmonic of the grid current to less than 0.002 A (0.1 %). Thus, the experiment effectively proves that the DC/AC inverter controlled by the proposed virtual oscillator can successfully eliminate the third-order harmonic component of the grid-injected current, and thereby improve the performance of the inverter.

V. CONCLUSIONS

In order to eliminate the undesirable third-order harmonics caused by VOC-based DC/AC inverters, an improved virtual oscillator has been proposed in this paper. The overall conclusions can be summarized as follows:

- 1) By reshaping the nonlinear current source of the traditional VOC, the proposed VOC-based DC/AC inverter successfully eliminates the third-order harmonic voltage.
- 2) Compared with the traditional VOC, the proposed VOC-based DC/AC inverter has a faster response speed.
- 3) Compared with the traditional VOC with notch filter, the proposed VOC-based DC/AC inverter has a faster synchronization speed in the islanded mode of operation.

The effectiveness of the proposed VOC has been fully verified via a 3 kW/3-phase/120 V experimental laboratory setup based on the dSPACE DS1202 platform.

TABLE I.

Symbol	Oscillator Parameters		
	Parameter	Value	U
C^*	Oscillator capacitance	0.1945	F
L	Oscillator inductance	52.087 E-6	H
α	Current source coefficeint	7.1975	A/V ³
σ	Conductance	10.7962	Ω^{-1}
K_i	Current feedback gain	0.152	A/A
K_v	Voltage scaling factor	120	V/V

TABLE II.

Symbol	DC/AC Inverter and Controller Parameters		
	Parameter	Value	U
U_{dc}	DC-link voltage	350	V
V_g	Grid voltage	120	V
K_p^θ	Phase proportional constant	-0.05	θ/θ
K_p^v	Voltage proportional constant	1	V/V
τ	Variable integral factor	5	θ/θ

Symbol	DC/AC Inverter and Controller Parameters		
	Parameter	Value	U
K_i^v	Voltage integral coefficient	1	V/V
L_1	Inverter-side filter inductor	1.2 E-3	H
R_1	Parasitic resistor	0.1	Ω
L_2	Grid-side filter inductor	1.2 E-3	H
R_2	Parasitic resistor	0.1	Ω
C_f	Filter capacitor	6 E-6	C
L_N	Grid inductor	2 E-3	H
R_L	Load resistance	22.12	Ω
L_L	Load inductance	14.4 E-3	H
f_s	Switching frequency	10	kHz

REFERENCES

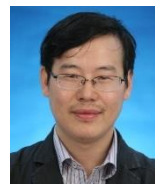
- [1] W. Wu, Y. Liu, Y. He, H. S. h. Chung, M. Liserre, F. Blaabjerg, "Damping Methods of Resonances Caused by LCL-Filter-Based Current-Controlled Grid-tied Power Inverters: an Overview", *IEEE Trans. on Ind. Electron.*, vol. 64, no. 9, pp. 7402 - 7413, Sept. 2017.
- [2] X. Wang, F. Blaabjerg, and W. Wu, "Modeling and Analysis of Harmonic Stability in an AC Power-Electronics-Based Power System", *IEEE Trans. on Power Electron.*, vol.29 no.12, pp. 6421 - 6432, Dec. 2014.
- [3] Y. Han, H. Li, P. Shen, E. A. A. Coelho and J. M. Guerrero, "Review of Active and Reactive Power Sharing Strategies in Hierarchical Controlled Microgrids," *IEEE Trans. on Power Electron.*, vol. 32, no. 3, pp. 2427-2451, March 2017.
- [4] K. De Brabandere, B. Bolsens, J. Van den Keybus, A. Woyte, J. Driesen and R. Belmans, "A Voltage and Frequency Droop Control Method for Parallel Inverters," *IEEE Trans. on Power Electron.*, vol. 22, no. 4, pp. 1107-1115, July 2007.
- [5] J. M. Guerrero, J. C. Vasquez, J. Matas, L. G. de Vicuna and M. Castilla, "Hierarchical Control of Droop-Controlled AC and DC Microgrids—A General Approach Toward Standardization," *IEEE Trans. on Ind. Electron.*, vol. 58, no. 1, pp. 158-172, Jan. 2011.
- [6] Y. Sun, X. Hou, J. Yang, H. Han, M. Su and J. M. Guerrero, "New Perspectives on Droop Control in AC Microgrid," *IEEE Trans. on Ind. Electron.*, vol. 64, no. 7, pp. 5741-5745, July 2017.
- [7] W. Yao, M. Chen, J. Matas, J. M. Guerrero, and Z.-M. Qian, "Design and Analysis of the Droop Control Method for Parallel Inverters Considering the Impact of the Complex Impedance on the Power Sharing," *IEEE Trans. on Industrial Electronics*, vol. 58, no. 2, pp. 576-588, Feb. 2011.
- [8] Q.-C. Zhong and Y. Zeng, "Universal Droop Control of Inverters With Different Types of Output Impedance," *IEEE Access*, vol. 4, pp. 702-712, 2016.
- [9] B. B. Johnson, S. V. Dhople, A. O. Hamadeh and P. T. Krein, "Synchronization of Nonlinear Oscillators in an LTI Electrical Power Network," *IEEE Trans. on Circuits and Systems I: Regular Papers*, vol. 61, no. 3, pp. 834-844, March 2014.
- [10] M. Sinha, F. Dörfler, B. B. Johnson and S. V. Dhople, "Synchronization of Liénard-type oscillators in heterogenous electrical networks," in *2018 Indian Control Conference (ICC)*, Kanpur, pp. 240-245, 2018.
- [11] S. V. Dhople, B. B. Johnson, F. Dörfler and A. O. Hamadeh, "Synchronization of Nonlinear Circuits in Dynamic Electrical Networks With General Topologies," *IEEE Trans. on Circuits and Systems I: Regular Papers*, vol. 61, no. 9, pp. 2677-2690, Sept. 2014.
- [12] S. V. Dhople, B. B. Johnson and A. O. Hamadeh, "Virtual Oscillator Control for voltage source inverters," in *2013 51st Annual Allerton Conference on Communication, Control and Computing*, Monticello, IL, pp. 1359-1363, 2013.
- [13] B. B. Johnson, S. V. Dhople, A. O. Hamadeh and P. T. Krein, "Synchronization of Parallel Single-Phase Inverters With Virtual Oscillator Control," *IEEE Trans. on Power Electron.*, vol. 29, no. 11, pp. 6124-6138, Nov. 2014.
- [14] B. B. Johnson, S. V. Dhople, J. L. Cale, A. O. Hamadeh and P. T. Krein, "Oscillator-Based Inverter Control for Islanded Three-Phase

- Microgrids," *IEEE Journal of Photov.*, vol. 4, no. 1, pp. 387-395, Jan. 2014.
- [15] B. B. Johnson, M. Sinha, N. G. Ainsworth, F. Dorfler, and S. V. Dhople, "Synthesizing virtual oscillators to control islanded inverters," *IEEE Trans. Power Electron.*, vol. 31, no. 8, pp. 6002-6015, Aug. 2016.
- [16] M. Sinha, F. Dorfler, B. B. Johnson, and S. V. Dhople, "Uncovering Droop Control Laws Embedded Within the Nonlinear Dynamics of Van der Pol Oscillators," *IEEE Trans. on Control of Network Systems*, vol. 4, no. 2, pp. 347-358, Jun. 2017.
- [17] M. Sinha, S. Dhople, B. Johnson, N. Ainsworth, and F. Dörfler, "Nonlinear supersets to droop control," in *Proc. of IEEE 16th Workshop Control Model. Power Electron.*, pp. 1-6, 2015.
- [18] M. Ali, H. I. Nurdin and J. E. Fletcher, "Output Power Regulation of a Virtual Oscillator Controlled Inverter," in *2018 IEEE 18th International Power Electronics and Motion Control Conference (PEMC)*, Budapest, pp. 1085-1090, 2018.
- [19] M. Ali, H. I. Nurdin and J. E. Fletcher, "Synthesizing Averaged Virtual Oscillator Dynamics to Control Inverters with an Output LCL Filter," in *46th Annual Conference of the IEEE Industrial Electronics Society (IECON 2020)*, Singapore, pp. 3265-3270, 2020.
- [20] M. Ali, H. I. Nurdin and J. Fletcher, "Dispatchable Virtual Oscillator Control for Single-Phase Islanded Inverters: Analysis and Experiments," *IEEE Transactions on Industrial Electronics*, in press.
- [21] D. Raisz, T. T. Thai and A. Monti, "Power Control of Virtual Oscillator Controlled Inverters in Grid-Connected Mode," *IEEE Trans. on Power Electron.* vol. 34, no. 6, pp. 5916-5926, June 2019.
- [22] P. Hazra, R. Hadidi, and E. Makram, "Dynamic study of virtual oscillator controlled inverter based distributed energy source," in *Proc. of 2015 North Amer. Power Symp.*, pp. 1-6.
- [23] G. Seo, M. Colombino, I. Subotic, B. Johnson, D. Groß, and F. Dorfler, "Dispatchable virtual oscillator control for decentralized inverter dominated power systems: Analysis and experiments," in *2019 IEEE Applied Power Electronics Conference and Exposition (APEC)*, pp. 561-566, 2019.
- [24] D. Groß, M. Colombino, J. Brouillon, and F. Dorfler, "The effect of transmission-line dynamics on grid-forming dispatchable virtual oscillator control," *IEEE Transactions on Control of Network Systems*, vol. 6, no. 3, pp. 1148-1160, 2019.
- [25] M. Colombino, D. Gross, J. Brouillon, and F. Dorfler, "Global phase and magnitude synchronization of coupled oscillators with application to the control of grid-forming power inverters," *IEEE Transactions on Automatic Control*, vol. 64, no. 11, pp. 4496-4511, 2019.
- [26] H. Yu, M. A. Awal, H. Tu, I. Husain and S. Lukic, "Comparative Transient Stability Assessment of Droop and Dispatchable Virtual Oscillator Controlled Grid-Connected Inverters," *IEEE Trans. on Power Electron.* vol. 36, no. 2, pp. 2119-2130, Feb. 2021.
- [27] J. Lin, "Virtual Oscillator Control of Distributed Power Filters for Selective Ripple Attenuation in DC Systems," *IEEE Trans. on Power Electron* (Early Access).
- [28] B. Johnson, M. Rodriguez, M. Sinha and S. Dhople, "Comparison of virtual oscillator and droop control," in *Proc. of 2017 IEEE 18th Workshop on Control and Modeling for Power Electron. (COMPEL)*, Stanford, CA, 2017, pp. 1-6.
- [29] M. Sinha, F. Dörfler, B. B. Johnson and S. V. Dhople, "Virtual Oscillator Control subsumes droop control," in *Proc. of 2015 American Control Conference (ACC)*, Chicago, IL, 2015, pp. 2353-2358.
- [30] M. A. Awal, H. Yu, H. Tu, S. M. Lukic and I. Husain, "Hierarchical Control for Virtual Oscillator Based Grid-Connected and Islanded Microgrids," *IEEE Trans. on Power Electron.*, vol. 35, no. 1, pp. 988-1001, Jan. 2020.
- [31] M. Lu, S. Dutta, V. Purba, S. Dhople and B. Johnson, "A Grid-compatible Virtual Oscillator Controller: Analysis and Design," in *2019 IEEE Energy Conversion Congress and Exposition (ECCE)*, Baltimore, MD, USA, pp. 2643-2649, 2019.
- [32] M. Lu, S. Dutta, V. Purba, S. Dhople and B. Johnson, "A Pre-synchronization Strategy for Grid-forming Virtual Oscillator Controlled Inverters," in *2020 IEEE Energy Conversion Congress and Exposition (ECCE)*, Detroit, MI, USA, pp. 4308-4313, 2020.
- [33] M. Lu, V. Purba, S. Dhople and B. Johnson, "Comparison of Droop Control and Virtual Oscillator Control Realized by Andronov-Hopf Dynamics," in *46th Annual Conference of the IEEE Industrial Electronics Society (IECON 2020)*, Singapore, pp. 4051-4056, 2020.
- [34] W. Wu, Y. He, F. Blaabjerg, "An LLCL- Power Filter for Single-phase Grid-tied Inverter," *IEEE Trans. on Power Electron.*, vol. 27, no. 2, pp. 782-789, Feb. 2012.

- [35] P. Jakobsen, "Introduction to the method of multiple scales," arXiv preprint arXiv:1312.3651, 2013.



Siyi Luo was born in Jiangxi, China, in 1996. He received the B.S. degree in software engineering and electrical engineering from East China Jiao Tong University, Nanchang, China, in 2018. He is currently working toward the M.S. degree in electrical engineering with Shanghai Maritime University, Shanghai, China. His current research interests include power electronics, distributed generation, renewable energy systems, and control of microgrid cluster systems.



Weimin Wu (M'16) received Ph.D. degrees in Electrical Engineering from the College of Electrical Engineering, Zhejiang University, Hangzhou, China, in 2005.

He worked as a research engineer in the Delta Power Electronic Center (DPEC), Shanghai, from July, 2005 to June, 2006. Since July, 2006, he has been a Faculty Member at Shanghai Maritime University, where he is currently a Full Professor in Department of Electrical Engineering. He was a Visiting Professor in the Center for Power Electronics Systems (CPES), Virginia Polytechnic Institute and State University, Blacksburg, USA, from Sept. 2008 to March. 2009. From Nov. 2011 to Jan. 2014, he was also a visiting professor in the Department of Energy Technology, Aalborg University, Denmark, working at the Center of Reliable Power Electronics (CORPE). He has coauthored over 100 papers and holds eight patents. His areas of interests include power converters for renewable energy systems, power quality, smart grid, and energy storage technology. Dr. Wu serves as an Associate Editor for the IEEE TRANSACTIONS ON INDUSTRY ELECTRONICS.



Eftichios Koutroulis (M'10-SM'15) was born in Chania, Greece, in 1973. He received the B.Sc. and M.Sc. degrees in electronic and computer engineering, in 1996 and 1999, respectively, and the Ph.D. degree in the area of power electronics and renewable energy sources (RES) from the School of Electronic and Computer Engineering, Technical University of Crete, Chania, Greece, in 2002. He is currently an Associate Professor in the School of Electrical and Computer Engineering, Technical University of Crete, where he also serves as Director of the Circuits, Sensors and Renewable Energy Sources laboratory. His research interests include power electronics, the development of microelectronic energy management systems for RES and the design of photovoltaic and wind energy conversion systems.



Henry Shu-Hung Chung (M'95-SM'03-F'16) received the B.Eng. and Ph.D. degrees in electrical engineering from the Hong Kong Polytechnic University, Kowloon, Hong Kong, in 1991 and 1994, respectively.

Since 1995, he has been with the City University of Hong Kong, Kowloon, where he is currently a Chair Professor in the Department of Electrical Engineering and the Director of the Center for Smart Energy Conversion and Utilization Research. His current research interests include renewable energy conversion technologies, lighting technologies, smart grid technologies, and computational intelligence for power electronic systems. He has edited one book, authored eight research book chapters, and over 460 technical papers including 200 refereed journal papers in his research areas, and holds 50 patents.

Dr. Chung was the Chair of the Technical Committee of the High-Performance and Emerging Technologies, IEEE Power Electronics Society in 2010-2014. He is currently Associate Editor of the IEEE Transactions on Power Electronics and the IEEE Journal of Emerging and Selected Topics in Power Electronics. He was Editor-in-Chief of the IEEE Power Electronics Letters 2014-2018. He has received numerous industrial awards for his invented energy saving technologies.



Frede Blaabjerg (S'86–M'88–SM'97–F'03) was with ABB-Scandia, Randers, Denmark, from 1987 to 1988. From 1988 to 1992, he got the PhD degree in Electrical Engineering at Aalborg University in 1995. He became an Assistant Professor in 1992, an Associate Professor in 1996, and a Full Professor of power electronics and drives in 1998. From 2017 he became a Villum Investigator. He is honoris causa at University Politehnica Timisoara (UPT), Romania

and Tallinn Technical University (TTU) in Estonia.

His current research interests include power electronics and its applications such as in wind turbines, PV systems, reliability, harmonics and adjustable speed drives. He has published more than 600 journal papers in the fields of power electronics and its applications. He is the co-author of four monographs and editor of ten books in power electronics and its applications.

He has received 33 IEEE Prize Paper Awards, the IEEE PELS Distinguished Service Award in 2009, the EPE-PEMC Council Award in 2010, the IEEE William E. Newell Power Electronics Award 2014, the Villum Kann Rasmussen Research Award 2014, the Global Energy Prize in 2019 and the 2020 IEEE Edison Medal. He was the Editor-in-Chief of the IEEE TRANSACTIONS ON POWER ELECTRONICS from 2006 to 2012. He has been Distinguished Lecturer for the IEEE Power Electronics Society from 2005 to 2007 and for the IEEE Industry Applications Society from 2010 to 2011 as well as 2017 to 2018. In 2019-2020 he served as a President of IEEE Power Electronics Society. He has been Vice-President of the Danish Academy of Technical Sciences.

He is nominated in 2014-2020 by Thomson Reuters to be between the most 250 cited researchers in Engineering in the world.